JMEPEG (2009) 18:787–792
DOI: 10.1007/s11665-009-9408-8

1059-9495/$19.00

Nitinol Embolic Protection Filters: Design Investigation by Finite Element Analysis

Michele Conti, Matthieu De Beule, Peter Mortier, Denis Van Loo, Pascal Verdonck, Frank Vermassen, Patrick Segers, Ferdinando Auricchio, and Benedict Verhegghe

(Submitted October 16, 2008; in revised form February 17, 2009)

The widespread acceptance of carotid artery stenting (CAS) to treat carotid artery stenosis and its effectiveness compared with surgical counterpart, carotid endarterectomy (CEA), is still a matter of debate. Transient or permanent neurological deficits may develop in patients undergoing CAS due to distal embolization or hemodynamic changes. Design, development, and usage of embolic protection devices (EPDs), such as embolic protection filters, appear to have a significant impact on the success of CAS. Unfortunately, some drawbacks, such as filtering failure, inability to cross tortuous high-grade stenoses, malpositioning and vessel injury, still remain and require design improvement. Currently, many different designs of such devices are available on the rapidly growing dedicated market. In spite of such a growing commercial interest, there is a significant need for design tools as well as for careful engineering investigations and design analyses of such nitinol devices. The present study aims to investigate the embolic protection filter design by finite element analysis. We first developed a parametrical computer-aided design model of an embolic filter based on micro-CT scans of the Angioguard™ XP (Cordis Endovascular, FL) EPD by means of the open source pyFormex software. Subsequently, we used the finite element method to simulate the deployment of the nitinol filter as it exits the delivery sheath. Comparison of the simulations with micro-CT images of the real device exiting the catheter showed excellent correspondence with our simulations. Finally, we evaluated circumferential basket-vessel wall apposition of a 4 mm size filter in a straight vessel of different sizes and shape. We conclude that the proposed methodology offers a useful tool to evaluate and to compare current or new designs of EPDs. Further simulations will investigate vessel wall apposition in a realistic tortuous anatomy.

Keywords Angioguard™, carotid artery stenting, embolic protection device, finite element analysis, nitinol, wall apposition

1. Introduction

Cardiovascular disease (CVD) is the main cause of death in Western countries. Each year CVD causes over 4.35 million deaths in Europe (accounting for 49% of all deaths in 2005) (Ref 1).

CVD is often related to atherosclerosis, a degeneration of the vessel wall which has the main consequence of narrowing the vessel lumen, i.e. a stenosis, leading to blood flow reduction or blockage.

This article is an invited paper selected from presentations at Shape Memory and Superelastic Technologies 2008, held September 21-25, 2008, in Stresa, Italy, and has been expanded from the original presentation.

Michele Conti and **Ferdinando Auricchio**, Universitá degli Studi di Pavia, Pavia, Italy; **Matthieu De Beule, Peter Mortier, Pascal Verdonck, Patrick Segers,** and **Benedict Verhegghe**, IBiTech, Institute of Biomedical Technology, Ghent University, Ghent, Belgium; **Denis Van Loo**, UGCT, Center for X-ray Tomography, Ghent University, Ghent, Belgium; and **Frank Vermassen**, Department of Vascular Surgery, Ghent University Hospital, Ghent, Belgium. Contact e-mail: michele.conti@unipv.it.

At present, the deployment of an intravascular stent has become a common and widely used minimally invasive treatment for stenotic arteries, including mainly coronary arteries but also peripheral stenotic vessels such as the carotid arteries.

ln recent years, carotid artery stenting (CAS) has emerged as a less invasive treatment as compared to the conventional surgical approach, carotid endarterectomy (CEA) (Ref 2), but the efficacy of CAS relative to surgery is still a matter of debate (Ref 3).

One major concern related to CAS is the possible distal embolization potentially leading to stroke or other severe neurological complications. Embolization is due mainly to the plaque debris and thrombi generated during the stenosis dilatation and stent apposition. Consequently, embolic protection devices (EPDs) have been developed to capture such released debris and appear to have a significant impact on the success of CAS (Ref 4-8).

EPDs can be classified in the following three categories (Ref 9):

- distal balloon occlusion;
- proximal balloon occlusion;
- embolic protection filters (EPFs).

The balloon occlusion systems block the flow in the internal carotid artery (ICA) and emboli are aspirated before balloon deflation and catheter removal, whereas EPFs maintain blood flow while emboli are captured.

Such a class of filters most often consists of a metallic basket-like structure coated with a membrane made of polymeric material containing numerous pores. Filters are usually mounted on a 0.014 in. (0.036 mm) guidewire, generally 30 mm proximal to a flexible tip and are delivered through a very small profile catheter (<3 French, i.e. 1 mm). During a CAS procedure, before the lesion dilatation and the stent apposition, the filter is opened in the ICA lumen distal to the target lesion, by withdrawing the delivery sheath. At the end of the CAS procedure, a retrieval catheter is advanced onto the guidewire to capture and remove the filter (Ref 10).

EPFs have both advantages and disadvantages with respect to balloon occlusion procedures. On one hand, EPFs have the advantage of preserving cerebral flow throughout the procedure while capturing embolic debris allowing distal perfusion and angiography during the CAS procedure. On the other hand, filters have disadvantages ranging from difficulty in navigating severely stenosed or tortuous vessels to possible incorrect filter apposition against the vessel wall (Ref 11, 12). Currently, several embolic filter designs are available on a fast growing dedicated market (Ref 11).

Because of the relevant differences in EPF designs, it is likely that there are situations in which individual EPFs may be better suited to avoid adverse events during CAS and, consequently, the investigation and the comparison of the performance of different EPFs can play a key role in the improvement of filtering outcomes and potentially on the complete CAS procedure.

Engineering investigation and computer models have shown the capability to provide useful information to understand the mechanics of cardiovascular devices, e.g. stents, and to improve device design (Ref 13-16). To the best of our knowledge, the available comparative investigations about advantages or roles that specific EPDs may have in CAS are mainly based on in vitro, ex vivo, or clinical studies (Ref 12, 17-20).

The purpose of this study is to use finite element analysis (FEA) in the design evaluation of basket-like embolic protection filters. In particular, we investigated the effects of sizing on circumferential basket-vessel wall apposition of a widely adopted embolic filter, i.e. the Angioguard™ XP (Cordis Endovascular, FL).

In order to achieve this purpose, we organized the study as follows:

- Using a script-based procedure, we created a 3D finite element model of the Angioguard™ XP taking into account several geometrical features (such as number of struts, strut diameter, filter length, filter diameter, etc.).
- To validate the model, we qualitatively compared the numerical prediction of a free filter expansion, i.e. as it exits out of the delivery sheath, with a micro-CT scan image of the real device deployment.
- To evaluate the circumferential basket-vessel wall apposition, we simulated the deployment of a 4 mm size Angioguard™ XP in a vessel having different sizes and shape.

2. Materials and Methods

2.1 Model Geometry

The Angioguard™ XP consists of a 0.014 in. (0.036 mm) guidewire with a nitinol basket frame enveloped by a porous polymeric membrane (Fig. 1). The current Angioguard™ XP basket sizes range from 4 to 8 mm in diameter in order to deploy within vessels with diameters ranging from 3.0 to 7.5 mm (Ref 11, 21).

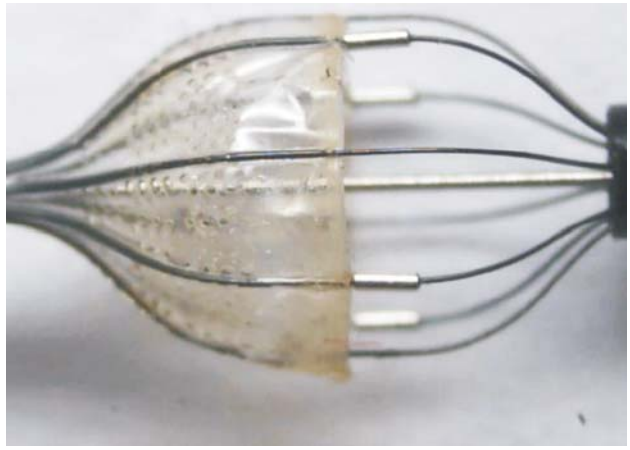

Fig. 1 The Angioguard™ XP embolic protection device

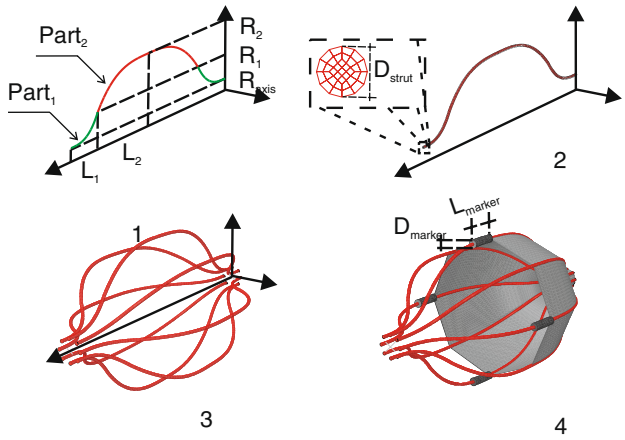

Fig. 2 Example of filter model generation in four steps

We used the in-house developed pyFormex software (version 0.6.5) (Ref 22) as a pre-processing tool to build a geometrical and finite element model of the Angioguard™ XP.

The model includes the following parts:

- filter struts defining the basket frame;
- membrane;
- markers.

The mesh generation procedure was defined by four essential steps (Fig. 2):

1. creation of path reproducing the shape of one filter strut;
2. sweeping of planar section along the defined path in order to create one 3D filter strut;
3. replication and rotation of the filter strut around the filter axis in order to create the whole basket frame;
4. definition of the whole model assembling the filter struts with the membrane and markers.

From a geometrical point of view, the model is defined by several parameters as depicted in Fig. 2 and reported in Table 1.

The pyFormex script-based mesh generation procedure allows the creation of a finite element model in a quick way facilitating parametrical finite element analyses; moreover, pyFormex generates a finite element mesh that can be easily imported into several commercial finite element solvers. In this study, we used ABAQUS/EXPLICIT 6.8 (Abaqus Inc., Providence, RI).

In order to assess accurately the value of the defined geometrical parameters, a micro-CT scan of a real device in open configuration was performed and the image was analyzed by Materialise miniMagics V12.0.5.1 (see Table 1).

2.2 Material Properties

The filter struts defining the basket frame are manufactured from nitinol, a nickel-titanium-based alloy showing the so-called superelastic effect (SE). A typical superelastic nitinol behavior is shown in Fig. 3 illustrating the ability to undergo large deformations (up to 6-8%) during loading and to fully recover such deformations during unloading. Clearly, the filter exploits this superelastic effect during both the delivery and retrieval phase, allowing the device to switch from a closed configuration to an open configuration and vice versa without experiencing plastic deformation.

In our simulations, nitinol superelasticity is modeled as a predefined user material in the ABAQUS/EXPLICIT 6.8 solver.

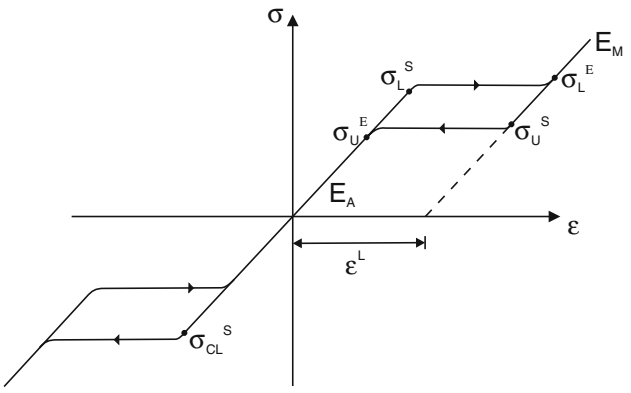

Fig. 3 Typical superelastic nitinol behavior

Table 1 Geometrical parameters of 4.0 mm filter model

Symbol	Description	Value
N_{struts}	Number of struts	8
R_{axis}	Distance of strut centerline from filter axis	0.3 mm
R_1	Filter radius (part 1)	0.68 mm
R_2	Filter radius (part 2)	1.02 mm
$R_{strut} = (R_{axis} + R_1 + R_2)$	Filter radius	2 mm
L_1	Filter length (part 1)	1.49 mm
L_2	Filter length (part 2)	2.76 mm
$L_{strut} = (2 * (L_1 + L_2))$	Filter length	8.5 mm
D_{strut}	Strut diameter	0.08 mm
$Membrane_{coverage}$	Percentage of filter coverage	50%
$Membrane_{th}$	Membrane thickness	0.02 mm
L_{marker}	Marker length	0.8 mm
D_{marker}	Marker diameter	0.22 mm

The polymeric porous membrane covering the filter frame was assumed to be manufactured in a Nylon-based material and having 0.02 mm thickness (Ref 14). The holes in the membrane were neglected.

The markers, attached to the nitinol frame to enhance filter radiopacity, were assumed to be manufactured by pure tantalum (Ref 23).

Table 2 reports the adopted material properties employed in the simulations.

2.3 Filter-Free Expansion

To validate the developed finite element model, we simulate the filter-free expansion, i.e. as it exits out of the delivery sheath. Consequently, the numerical analysis of this free expansion of filter is a non-linear problem involving large deformation and contact problems in the numerical analysis.

For this purpose, large deformation analyses were performed using the ABAQUS/EXPLICIT solver, particularly quasi-static procedures were used assuming that inertia forces do not dominate/change the analysis. Kinetic energy was monitored to ensure that the ratio of kinetic energy to internal energy remains less than 10%. Moreover, a mass scaling strategy was used to reduce computational cost.

All finite element simulations were carried out on an in-house built low-cost, high-performance computing cluster (Ref 24).

The delivery sheath was assumed to be a straight rigid cylinder having a diameter equal to 1.06 mm and a length of 15 mm.

Table 2 Material properties used in the simulations

Nitinol (Ref 28)		
E_A	Austenite Young's modulus	35877 MPa
ν_A	Austenite Poisson's ratio	0.33
E_M	Martensite Young's modulus	24462 MPa
ν_M	Martensite Poisson's ratio	0.33
ε^L	Transformation strain	0.0555
$(d\sigma/dT)_L$	Loading temperature derivative of stress	0 MPa/°C
σ^S_L	Loading start of transformation stress	489 MPa
σ^E_L	Loading end of transformation stress	572 MPa
T_0	Temperature	22 °C
$(d\sigma/dT)_U$	Unloading temperature derivative of stress	0 MPa/°C
σ^S_U	Unloading start of transformation stress	230 MPa
σ^E_U	Unloading end of transformation stress	147 MPa
σ^E_{CL}	Start of transformation stress (compression)	…
ρ_{strut}	Density (a)	6.5 g/cm^3
Nylon (Ref 14)		
E_{membr}	Modulus of elasticity	920 N/mm^2
ν_{membr}	Poisson's ratio	0.4
ρ_{membr}	Density	1.1 g/cm^3
Tantalum (Ref 23)		
E_{marker}	Modulus of elasticity	179000 MPa
ν_{marker}	Poisson's ratio	0.35
ρ_{marker}	Density	16.6 g/cm^3

(a) http://www.shape-memory-alloys.com/data_nitinol.htm

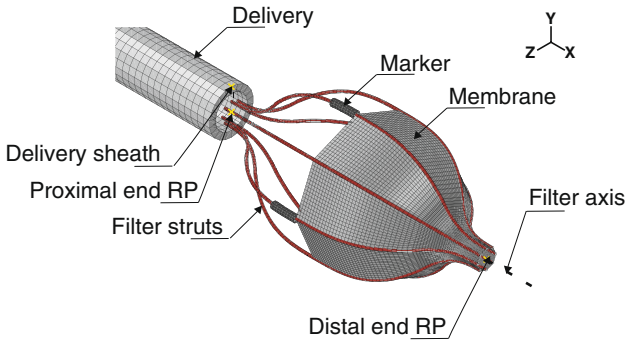

Fig. 4 Finite element model of Angioguard™ XP and part of the delivery sheath

The parts defining filter/catheter systems (see Fig. 4) were modelled as follows:

- *filter struts*: 33,792 three-dimensional 8-node brick 'reduced-integration' elements (C3D8R);
- *membrane*: 8320 three-dimensional 4-node quadrilateral membrane elements with reduced integration (M3D4R);
- *markers*: 1296 three-dimensional 8-node brick 'reduced-integration' elements (C3D8R);
- *catheter*: 3806 three-dimensional 4-node bilinear quadrilateral rigid elements (R3D4).

Mesh tie constraints of type surface-to-surface were applied to tie the markers and the membrane to the filter struts.

Furthermore, the filter frame struts are tied to marker bands defining the relative movement of the filter ends with respect to the guidewire (Ref 21), particularly the proximal marker band is fixed to the guidewire while the distal marker band is free to slip along the guidewire. Therefore, mesh tie constraints, type rigid body, are imposed between the nodes lying on each filter frame end and the predefined reference points. Boundary conditions are then applied to the reference points (RPs) to realistically simulate the movement of the marker bands. In particular, at the proximal end RP, all the degrees of freedom were constrained; at the distal end RP, only displacement along filter axis and rotations were allowed.

The analysis strategy assumes that the filter frame deformation during deployment is comparable to the deformation during the filter frame insertion into the delivery sheath. Consequently, a progressive rigid translation along the filter axis is imposed to the delivery sheath in order to induce the necessary filter deformation to switch from the open configuration (filter out of delivery sheath) to the closed configuration (filter within the delivery sheath).

A frictionless general contact algorithm has been used in order to handle the interactions between the filter frame and the deployment sheath. In this case, the membrane elements were excluded from the contact strategy in order to simplify the simulations assuming that it has a minor role in the overall filter deployment/retrieval mechanics.

2.4 Circumferential Basket-Vessel Wall Apposition

In order to evaluate the circumferential basket-vessel wall apposition, we carried out the simulations of a filter deploying in a straight vessel modelled as a rigid cylinder having different sizes and shape. In particular, two different scenarios were investigated: (i) filter expansion in three circular vessels having

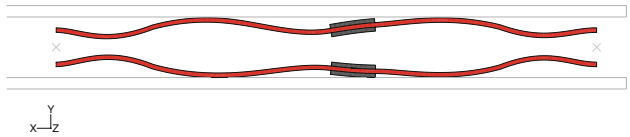

Fig. 5 Longitudinal cut view of the filter frame in the delivery sheath

respectively 3.0, 3.25, and 3.5 mm diameter as suggested by the manufacturer for a 4 mm size filter (Ref 21); (ii) filter expansion in two oval vessels having both 1.5 mm major semi axis and respectively an ovality* of 0.85 and 0.75.

Preliminary simulations showed that, in the analyzed case, final filter/vessel configuration is not influenced by the deploying mode and consequently the interaction between filter and sheath has not been taken into account.

We defined a two-step simulation strategy as follows: (i) filter diameter reduction is obtained by elongating the basket frame by appropriate axial displacement boundary conditions to the distal end RP, only self contact of membrane was included in this step; (ii) previous boundary conditions are deactivated allowing the filter re-expansion and a global contact algorithm was included allowing the filter/vessel interaction.

The effect of blood flow pressure acting on the filter membrane was included in the analyses applying a uniform pressure of 8.80 mmHg on the inner surface of the membrane (Ref 25).

Circumferential basket-vessel wall apposition was evaluated in terms of gap between the vessel lumen and the circumferential area covered by the filter.

In order to keep the computational cost acceptable and to minimize the impact of the membrane mesh on the gap measurement, a final membrane mesh of M3D4R 24960 elements was chosen by a preliminary mesh sensibility analysis about filter deployment simulation in the 3 mm circular vessel (a finer membrane mesh—29,120 elements—results in a 5.4% gap measurement differing 6% compared to the 5.7% gap obtained with the coarser mesh—24,960 elements).

3. Results

3.1 Filter-Free Expansion

The simulation of the filter-free expansion showed that the basket-frame configuration experiences a severe change. The radial compression of the filter frame is accomplished by an axial elongation bringing the diameter to a final value of 0.96 mm when the filter is completely inserted into the sheath as shown in Fig 5. Moreover, the filter frame experiences a radial deformation that is not uniform along the filter length, resulting in non-uniform adhesion between the strut and the delivery sheath wall.

Comparing the previously described adopted mesh to a finer one (i.e. 67,584, 33,024, and 2,592 elements respectively for filter struts, membrane, and markers) showed a negligible divergence (i.e. difference in maximum axial elongation less than 1%).

*Ovality being defined as the change in cross section roundness and defined as $O = b/a$, where a is cross section semi-major axis length and b is cross section semi-minor axis length.

Moreover, Fig. 6 shows a good qualitative agreement between the numerical results and the micro-CT image of the partially deployed Angioguard™ XP.

3.2 Circumferential Basket-Vessel Wall Apposition

Simulations of the filter deployment in the straight vessel showed that the filter is not able to completely cover the vessel lumen and gaps are present between the vessel wall and the membrane (see Fig. 7), confirming the experimental results recently reported by Sieworek et al. (Ref 26).

As reported in Table 3, the vessel size seems to have a minor impact on the circumferential basket-vessel wall apposition which is in contrast to the impact of the vessel shape. In fact, an increase in the vessel ovality dramatically influences the gap while a change in the vessel diameter does not significantly modify the gap area.

Consequently, the simulations of filter deployment in the straight rigid vessel suggest that, in this case, filter malapposition is caused by inability of the filter struts to accomplish the vessel asymmetry.

4. Limitations

The filter-free expansion simulation showed qualitative agreement with micro-CT images but limitations pertaining to the frictionless contact between the filter and the delivery sheath are present.

Clearly, the assumption of a uniform pressure distribution along the filter membrane should be improved using more accurate and realistic values achieved, for example, by experiments and computational fluid dynamics analyses.

Material properties of the filter components should also be derived from experimental data to define the mechanical properties more accurately.

The major limitation of this study is the rigid body assumption for the vessel. In reality, the radial outward force of the filter is likely to reshape the vessel and this effect can consequently influence the filter-vessel wall apposition. However, modeling filter apposition in a realistic vessel (i.e. internal carotid artery) introduces substantial computational challenges, such as the incorporation of the variability of the constitution and mechanical properties of the diseased arterial wall, and should be accomplished by adequate experimental validation. This challenge is considered to be beyond the scope of this preliminary investigation.

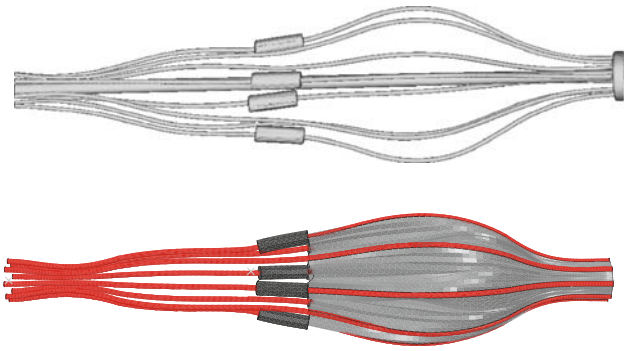

Fig. 6 Partially deployed filter: microCT image (top panel); numerical simulation (bottom panel)

5. Conclusions

In this study, we proposed and validated a finite element model in order to investigate the basket-like design of an embolic protection filter device. In particular, the circumferential filter/vessel wall apposition was numerically evaluated confirming the inability of the filter to completely adapt to asymmetric vessels.

Clearly, this study needs to be considered as a preliminary proof of concept of the use of finite element based modeling

Table 3 Numerical results of filter/vessel wall apposition

	Filter size, mm—Ovality				
	3.5-0.0	**3.25-0.0**	**3.0-0.0**	**3.0-0.85**	**3.0-0.75**
Gap (% of vessel lumen)	5.7	4.7	5.7	8.7	14.7

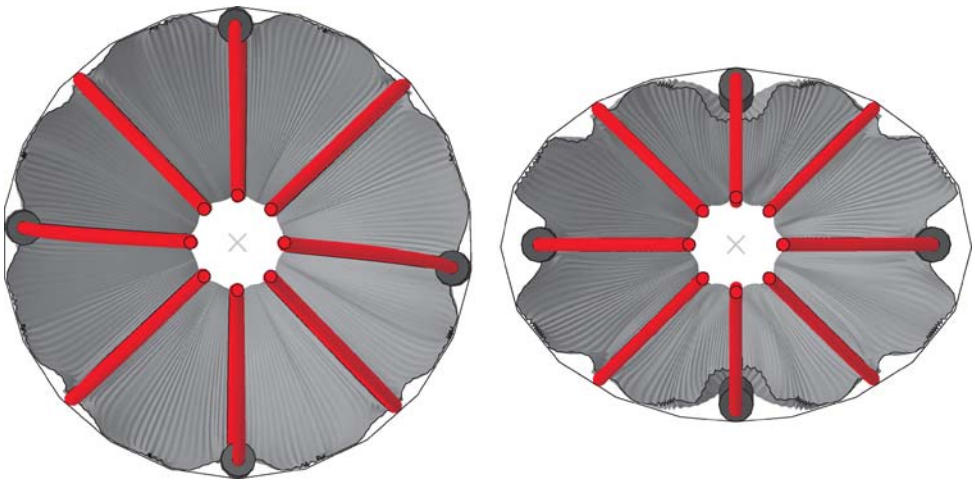

Fig. 7 A 4 mm size filter deployed in a 3 mm circular vessel (on the left) and in 3 mm vessel having 0.75 ovality (on the right)

strategies to investigate and understand the mechanics of embolic protection filters. The proposed model is a base to further investigate the impact of design parameters (filter length, diameter, number of struts, etc.) on filter mechanics (flexibility, radial strength, etc.) and the filter apposition in a more realistic tortuous anatomy taking also into account vessel wall material properties.

Finally, we finally conclude that the proposed methodology could be useful to evaluate and to compare current or new designs of EPDs in the early design phase as recently recommended by the FDA (Ref 27).

References

1. S. Petersen, V. Peto, M. Rayner, J. Leal, R. Luengo-Fernandez, and A. Gray, European Cardiovascular Disease Statistics, BHF London, 2005
2. M.H. Wholey, N. Al-Mubarek, and M.H. Wholey, Updated Review of the Global Carotid Artery Stent Registery, *Catheter. Cardiovasc. Interv.*, 2003, **60**, p 259–266
3. A.J. Furlan, Carotid-Artery Stenting—Case Open or Closed? *N. Engl. J. Med.*, 2006, **355**(16), p 1726–1729
4. N. Al-Mubarak, G.S. Roubin, J.J. Vitek, S.S. Iyer, G. New, and M.B. Leon, Effect of the Distal Balloon Protection System on Microembolization During Carotid Stenting, *Circulation*, 2001, **104**, p 1999–2002
5. J.S. Yadav, M.H. Wholey, R.E. Juntz, P. Fayad, B.T. Katzen, G.J. Mishkel, T.K. Bajwa, P. Whitlow, N.E. Strickman, M.R. Jaff, J.J. Popma, D.B. Snead, D.E. Cutlip, B.G. Firth, and K. Ouriel, Protected Carotid Artery Stenting Versus Endarterectomy in High-Risk Patients, *N. Engl. J. Med.*, 2004, **351**, p 1493–1501
6. P.P. Goodney, M.L. Schermerhorn, and R.J. Powell, Current Status of Carotid Artery Stenting, *J. Vasc. Surg.*, 2006, **43**, p 406–411
7. CaRESS Steering Committee, Carotid Revascularization Using Endarterectomy or Stenting Systems (CaRESS) Phase I Clinical Trial: 1-year Results, *J. Vasc. Surg.*, 2005, **42**, p 213–219
8. M.H. Yen, D.S. Lee, S. Kapadia, R. Sachar, D.L. Bhatt, C.T. Bajzer, and J.S. Yadav, Symptomatic Patients Have Similar Outcomes Compared with Asymptomatic Patents After Carotid Artery Stenting with Emboli Protection, *Am. J. Cardiol.*, 2005, **95**, p 297–300
9. M.K. Eskandari, S.F. Najjar, J.S. Matsumura, M.R. Kibbe, and M.D. Morasch, Technical Limitations of Carotid Filter Embolic Protection Devices, *Ann. Vasc. Surg.*, 2007, **21**, p 403–407
10. F. Fanelli, M. Bezzi, E. Boatta, and R. Passariello, Techniques in Cerebral Protection, *Eur. J. Radiol.*, 2006, **60**, p 26–36
11. K. Kasirajan, P.A. Schneider, and K.C. Kent, Filter Devices for Cerebral Protection During Carotid Angioplasty and Stenting, *J. Endovasc. Ther.*, 2003, **10**, p 1039–1045
12. G.M. Siewiorek, M.H. Wholey, and E.A. Finol, In Vitro Performance Assessment of Distal Protection Devices for Carotid Artery Stenting: Effect of Physiological Anatomy on Vascular Resistance, *J. Endovasc. Ther.*, 2007, **14**(5), p 712–724
13. F. Auricchio, M. Di Loreto, and E. Sacco, Finite Element Analysis of a Stenotic Artery Revascularization Through Stent Insertion, *Comput. Methods Biomech. Biomed. Eng.*, 2000, **0**, p 1–15
14. M. De Beule, P. Mortier, S.G. Carlier, B. Verhegghe, R. Van Impe, and P. Verdonck, Realistic Finite Element-Based Stent Design: The Impact of Balloon Folding, *J. Biomech.*, 2008, **41**(2), p 383–389
15. C. Lally, F. Dolan, and P. Prendergast, Cardiovascular Stent Design and Vessel Stresses: A Finite Element Analysis, *J. Biomech.*, 2005, **38**(8), p 1574–1581
16. P. Mortier, M. De Beule, S.G. Carlier, R. Van Impe, B. Verhegghe, and P. Verdonck, Numerical Study of the Uniformity of Balloon-Expandable Stent Deployment, *J. Biomech. Eng.*, 2008, **130**(2), p 021018
17. S. Muller-Hulsbeck, T. Jahnke, C. Liess, C. Glass, F. Paulsen, J. Grimm, and M. Heller, In Vitro Comparison of Four Cerebral Protection Filters for Preventing Human Plaque Embolization During Carotid Interventions, *J. Endovasc. Ther.*, 2002, **9**(6), p 793–802
18. S. Muller-Hulsbeck, T. Jahnke, C. Liess, C. Glass, J. Grimm, and M. Heller, Comparison of Various Cerebral Protection Devices Used for Carotid Artery Stent Placement: An In Vitro Experiment, *J. Vasc. Interv. Radiol.*, 2003, **14**(5), p 613–620
19. S. Muller-Hulsbeck, P. Stolzmann, C. Liess, J. Hedderich, F. Paulsen, T. Jahnke, and M. Heller, Vessel Wall Damage Caused by Cerebral Protection Devices: Ex Vivo Evaluation in Porcine Carotid Arteries, *Radiology*, 2005, **235**(2), p 454–460
20. R.J. Powell, C. Alessi, B. Nolan, E. Rzucidlo, M. Fillinger, D. Walsh, M. Wyers, R. Zwolak, and J.L. Cronenwett, Comparison of Embolization Protection Device Specific Technical Difficulties during Carotid Artery Stenting, *J. Vasc. Surg.*, 2006, **44**, p 56–61
21. Instructions for use Angioguard XP™ Emboli Capture Guidewire system. www.cordislabeling.com/pdf/24408544_3.pdf. Accessed 16 March 2009
22. http://pyFormex.berlios.de. Accessed 16 March 2009
23. http://www.cabot-corp.com. Accessed 16 March 2009
24. http://bumps.ugent.be/bumper. Accessed 16 March 2009
25. J.M. Hendriks, J.D. Zindler, A. van der Lugt, P. Pattynama, M. van Sambeek, J. Bosch, and L. van Dijk, Embolic Protection Filters for Carotid Artery Stenting: Differences in Flow Obstruction Depending on Filter Construction, *J. Endovasc. Ther.*, 2006, **13**(1), p 47–50
26. G.M. Sieworek, M.K. Eskandari, and E.A. Finol, The Angioguard™ Embolic Protection Device, *Expert Rev. Med. Devices*, 2008, **5**(3), p 287–296
27. Guidance for Industry and FDA Staff, Coronary and Carotid Embolic Protection Devices—Premarket Notification [510(k)] Submissions. http://www.fda.gov/cdrh/ode/guidance/1658.html. Accessed 16 March 2009
28. A.R. Pelton, J. DiCello, and S. Miyazaki, Optimisation of Processing and Properties of Medical Grade Nitinol Wire, *Minim. Invasive Ther. Allied Technol.*, 2000, **9**(1), p 107–118